RMetS
Royal Meteorological Society

Notes and Correspondence
Influence of atmospheric and sea surface temperature on the size of hurricane *Catarina*

Raluca Radu,* Ralf Toumi and Jared Phau
Imperial College London, UK
*Correspondence to: R. Radu, Imperial College London, Space and Atmospheric Physics, South Kensington Campus, London, SW7 2AZ, UK. E-mail: raluca.radu@imperial.ac.uk

The factors that influence the size of tropical cyclones (TCs) are not completely understood. High-resolution numerical simulations of hurricane *Catarina* in the South Atlantic indicate that the TC size increases proportionally to the surface latent heat flux, when atmospheric and sea surface temperature (SST) are increased. The TC size is defined as the area enclosed by three wind thresholds: gale-force winds, damaging-force winds and hurricane-force winds. The enlargement increases sharply with the wind threshold. Depending on the wind threshold, the area can increase by more than an order of magnitude when air and sea temperature are both increased by 2 °C. There is a clear linear relationship between the size increase and the latent heat flux during the TC lifetime. The size effect is driven initially by the enhanced air–sea moisture contrast and the surface winds become predominant only in the later stages. Temperature changes may therefore have a profound impact on cyclone size.

Key Words: tropical cyclone size; latent heat flux; temperature increase

Received 12 January 2013; Revised 21 July 2013; Accepted 23 July 2013; Published online in Wiley Online Library 9 January 2014

1. Introduction

The size of a tropical cyclone is one of the most important characteristics when considering impacts (storm surge, precipitation amount, area hit by damaging winds or area threatened at landfall). The geometric size of a tropical cyclone (TC), an indication of the storm horizontal dimension, is often measured by the average distance from the storm centre to the region of maximum wind speed (radius of maximum winds) or by average distance from the TC centre to the outermost closed isobar (Demuth *et al.*, 2006). Weatherford and Gray (1988a) defined the 'inner-core' starting from cyclone centre to 1 ° latitude radius, while the 'outer-core' was the region between radii of 1 and 2.5 ° latitudes. Other methods of determining a tropical cyclone size include measuring the radius at which its relative vorticity field decreases to 1×10^{-5} s^{-1} from its centre (Liu and Chan, 1999). TC size has been shown to depend on many factors. Merrill (1984) finds a weak correlation between intensity and size and that the changes in TC size are related to increase convergence of the angular momentum. Weatherford and Gray (1988b) showed that TC size measured by radial extent of gale-force winds is weakly correlated with the TC intensity. The size of a mature TC may be determined by the size of the TC at formation (Emanuel, 1986; Rotunno and Emanuel, 1987; Cocks and Gray, 2002). Kimball and Mulekar (2004) and Hill and Lackmann (2009) found that increased moisture in a TC environment enhances the outer rainbands leading to a larger storm. Dean *et al.* (2009) suggested that TC size is a function of the precursor disturbance. Stovern and Ritchie (2012) explored the influence of atmospheric temperature on TC size in an idealized framework where the virtual atmospheric temperature profile was increased or decreased relative to constant 29 °C sea surface temperature (SST), and they showed that cooler atmosphere led to increased surface moisture fluxes, higher potential vorticity and outer rainbands generation and larger wind field. Recently, Rozoff *et al.*(2012) notice that latent heating outside the primary eyewall promotes the secondary eyewall formation leading to expansion of the outer wind field which in turn determines the TC size. Related to our study, Xu and Wang (2010a) emphasize the importance of the surface moist entropy flux on the TC size. Their results showed that surface entropy flux in the outer eyewall contributes to the increase of the activity of spiral rainbands, leading to the increase of the TC inner-core size, in agreement with the previous studies (Hill and Lackmann, 2009; Wang, 2009).

Here we show how the TC size is affected by the atmospheric temperature and SST changes in high-resolution simulations of a real hurricane. Hurricane *Catarina*, which is the first hurricane in the South Atlantic, was chosen as case-study because it raises concerns about the potential effects of climate change in a region usually free of hurricanes (Evans and Braun, 2012). If hurricanes are an emerging phenomenon in new regions, then our sensitivity study performed here will have additional relevance. The experimental design tests the sensitivity of the TC size to perturbations in the initial and boundary temperature. In this respect the main purpose is to investigate the influences of higher temperature variations in determining the simulated TC size.

2. Model and experimental set-up

This study utilizes the Advanced Research Weather Research and Forecast model (ARW-WRF version 3.2.1; Skamarock *et al.*, 2005) to simulate a real *Catarina*. All experiments used the following

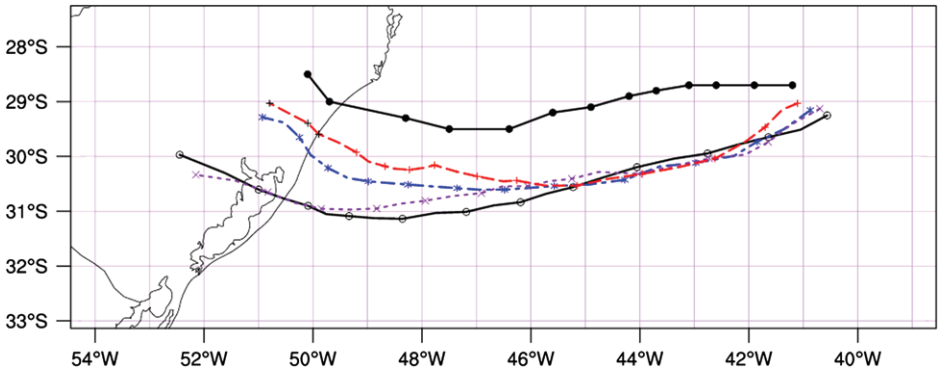

Figure 1. Tracks of hurricane *Catarina* starting at 1200 UTC on 25 March 2004 after 84 integration hours, corresponding with tropical storm development stage: best track (solid line and filled circles), the control simulation track (CTL, solid line and open circles) and the sensitivity simulation tracks with SST and atmospheric temperature profile increased by 1 °C (T1, dot-dashed line and asterisks), by 2 °C (T2, dashed line and plus signs), then with increased SST by 1 °C and the atmospheric temperature profile by 2 °C (T12, dotted line and crosses).

set-up: Kain–Fritsch cumulus parametrization scheme (Kain and Fritsch, 1993; Kain, 2004), Thompson scheme for parametrization of microphysical processes, the Rapid Radiative Transfer Model scheme (Mlawer *et al.*, 1997) to estimate the effects of long-wave radiation and Dudhia (1989) implementation for short-wave radiation. The surface layer uses similarity scheme based on Monin–Obukhov with Carslon–Boland viscous sub-layer and standard similarity functions, along with Yonsei University scheme (Hong *et al.*, 2006) for parametrization of processes in the planetary boundary layer. Some experiments using slightly different domains and various model parametrization schemes have been previously performed and for each of the cases similar results were obtained, showing that the outcome of this work is not sensitive to the model set-up.

Our experiments used ECWMF Reanalyses ERA-Interim (Dee *et al.*, 2011) atmospheric fields at 1.5° horizontal resolution as initial and lateral boundary conditions for the WRF model integration. The domain is located between −34.27 to −21.55 °S and −54.30 to −31.41 °W with a horizontal resolution of 3.3 km. In order to achieve this resolution, the domain was nested within two larger domains with 30 and 10 km horizontal resolution. At the highest horizontal resolution, no cumulus parametrizations were used. There are 42 vertical levels, with resolution increased at the bottom and top, and a model top of 50 hPa. All the experiments started at 0000 UTC on 22 March 2004 and ran for 10 days.

Four model simulations to study the sensitivity of the TC size to perturbations of the SST and atmospheric temperature were performed. In each experiment the SST and the atmospheric temperature profiles used as initial conditions and 6 hourly lateral boundary conditions were perturbed as follows: in the control experiment (CTL), the SST and the atmospheric temperature were not changed, while in the sensitivity experiments the SST and the atmospheric temperature profile were both increased by 1 °C (T1), and by 2 °C (T2). A uniform profile change aims to maintain the atmospheric vertical stability in the column. In the last sensitivity experiment (T12), the SST was increased by 1 °C and the air temperature by 2 °C. The other variables in the initial and boundary conditions, including relative humidity, were kept the same in all experiments. The specific humidity increases in T1, T2 and T12 as consequence of increasing the water vapour saturation.

3. Results

3.1. Storm position

Hurricane *Catarina* formed in unusual large-scale conditions with relatively cool SST of about 25 °C and low wind shear in the presence of a dipole blocking system, as described by McTaggart-Cowan *et al.*(2006). It should be noted that the historical temperature variation has been about 1 °C higher in this region, similar to our T1 experiment (Pezza *et al.*, 2009).

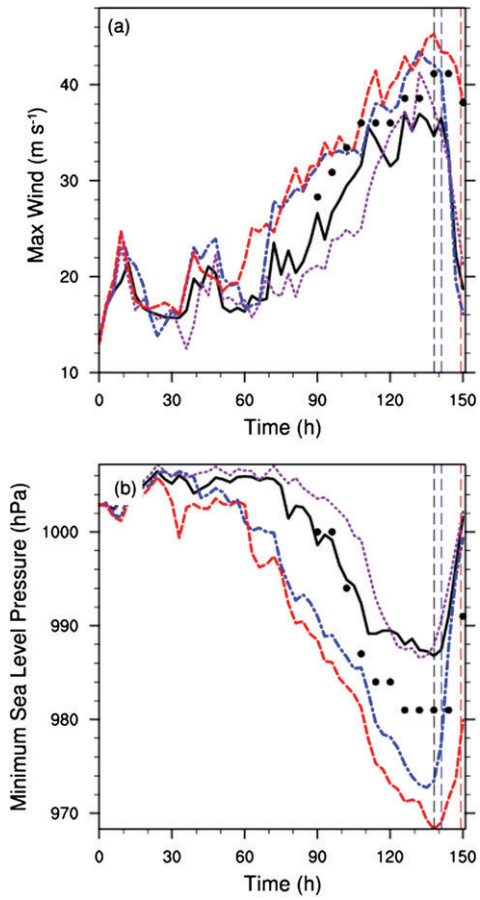

Figure 2. Simulated intensity for hurricane *Catarina* with WRF model, given by (a) the maximum wind speed (m s^{-1}) time evolution and (b) by minimum sea level pressure (hPa), for the control (CTL, solid line) and the sensitivity experiments with increased SST and atmospheric temperature profile: T1 (dot-dashed), T2 (dashed) and T12 (dotted). The black points represent the observed values and the vertical dashed lines are the landfall times.

Figure 1 shows the best track and the simulated tracks of hurricane *Catarina*, starting from the tropical storm stage. Tracks are displayed for the observed path (provided by the International Best Track and Archive for Climate Stewardship, IBTraCS; Knapp *et al.*, 2010), the control (CTL) and the perturbed simulations (T1, T2, T12), where the location of minimum of sea level pressure represents the central position of the storm. The simulated tracks follow the observed track and the landfall location closely. We notice some deviation of the tracks in the sensitivity runs compared to the control. There is a northward shift of about 1 °

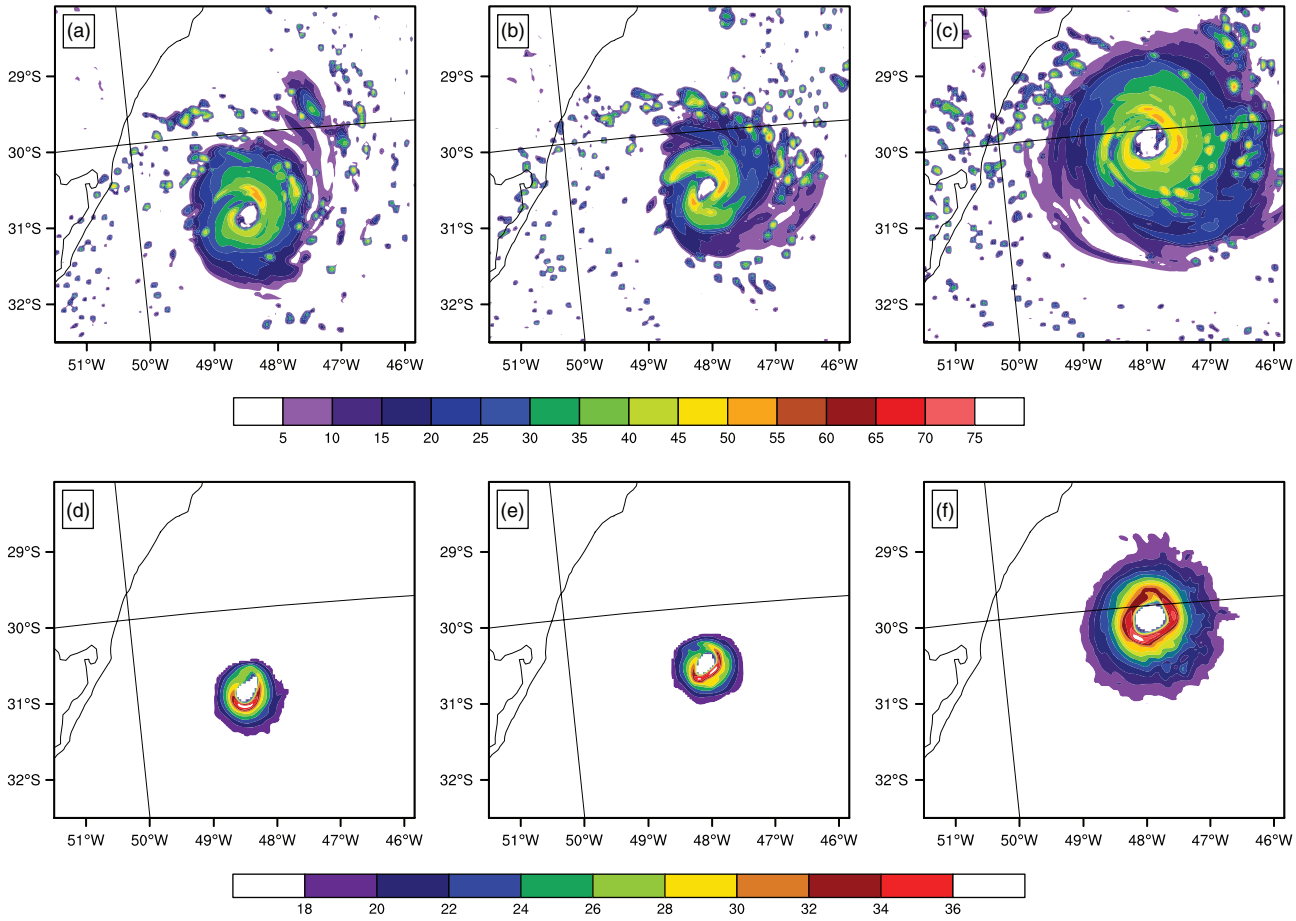

Figure 3. (a, b, c) Maximum synthetic reflectivity (dBZ) and (d, e, f) gale-force wind contours (m s^{-1}), for (a, d) CTL, for (b, e) T12, and (c, f) for T2 at 0900 UTC on 27 March 2004.

latitude in T1 and 1.5 ° latitude in T2 towards a region of higher SST nearer the coast (Fisher, 1958; Pezza *et al.*, 2009).

3.2. *Intensity: maximum wind speed*

Figure 2 shows the time evolution of the cyclone intensity in terms of maximum wind speed and minimum sea level pressure in the control and sensitivity experiments. After approximately 60 h the storm progressively starts to develop in all four experiments, showing similar patterns in terms of intensification with a maximum wind speed of 38 m s^{-1} and a minimum sea level pressure of 987 hPa in the control simulation. The maximum wind speed at peak intensity (approximately at 0000 UTC on 28 March 2004) estimated from the satellite data was around 44 m s^{-1}, while the minimum sea level pressure was about 972 hPa (McTaggart-Cowan *et al.*, 2006). There is an increase in maximum wind speed of about 18 and 20% in the T1 and T2 experiment, respectively.

3.3. *Cyclone size*

Here we define the size of the tropical cyclone in terms of area enclosed by different wind thresholds: gale-force winds (34 knots or 17.5 m s^{-1}), damaging-force winds (50 knots or 25.7 m s^{-1}), hurricane-force winds (64 knots or 33 m s^{-1}) and the radius where the maximum wind speed decreases to half. Figure 3 shows the simulated maximum reflectivity (dBZ, first row) and gale-force wind (m s^{-1}, second row) at 0900 UTC on 27 March 2004 close to the moment of maximum storm intensity. The T1 and T2 sensitivity simulations present an increase of the TC size for these diagnostic variables. The temporal evolution of the cyclone also shows enhanced size effects in the simulations. Figure 4 shows the time evolution of the area enclosed by the different wind thresholds. The area defined by the wind thresholds is larger in T1 and T2 than the control at all times. In T12 the TC size fluctuates above and below the control run during the lifetime of the cyclone. We can also compare lifetime average enhancement of the areas of the gale-force, damaging-force and hurricane-force wind for T2 and T1 against the control simulation. In T2 the average area of gale-force wind is 3.5 times larger than in the control, in T1 it is 2.8 larger than in the control, while the area of gale-force wind in T12 is very close to the control. As expected, the size effect becomes more pronounced for more extreme winds. We notice the size increases for the hurricane-force wind threshold, showing a nonlinear increase of the maximum wind area with the temperature increase. In T2 the lifetime average area is about 25 times larger than the control, while in T1 the average area is about 13 times larger than the control area for hurricane-force winds. However, T12 shows the smallest average enhancement of only 30% during the cyclone lifetime. The growth in size is smaller if we consider only the maximum area during the cyclone lifetime. For example, in the case of hurricane-force winds the maximum area increases by a factor of 12 and 18 for T1 and T2, respectively.

In order to separate the change in intensity from the change in size, we calculated the radius at which the tangential wind speed decreases to half of its maximum value. Figure 4(d) shows that for T1 and T2, the radius increases by up to 1.5 and 2 times respectively compared to the control. Figure 5 shows the azimuthal mean of the tangential wind speed at the surface at the time of the maximum intensity. The relationship of size with maximum intensity is not straightforward. On the other hand T1 and T2 both have larger maximum intensity and are bigger than the control. This appears like an upward shift or linear relationship in the wind profile in Figure 5. However, T12 has a larger maximum wind yet is slightly smaller than the control for strong winds. T1 and T2 have similar maxima yet T2 is bigger. Figure 6 shows the vertical distribution of the tangential wind speed. Although the surface winds between T1 and T2 are

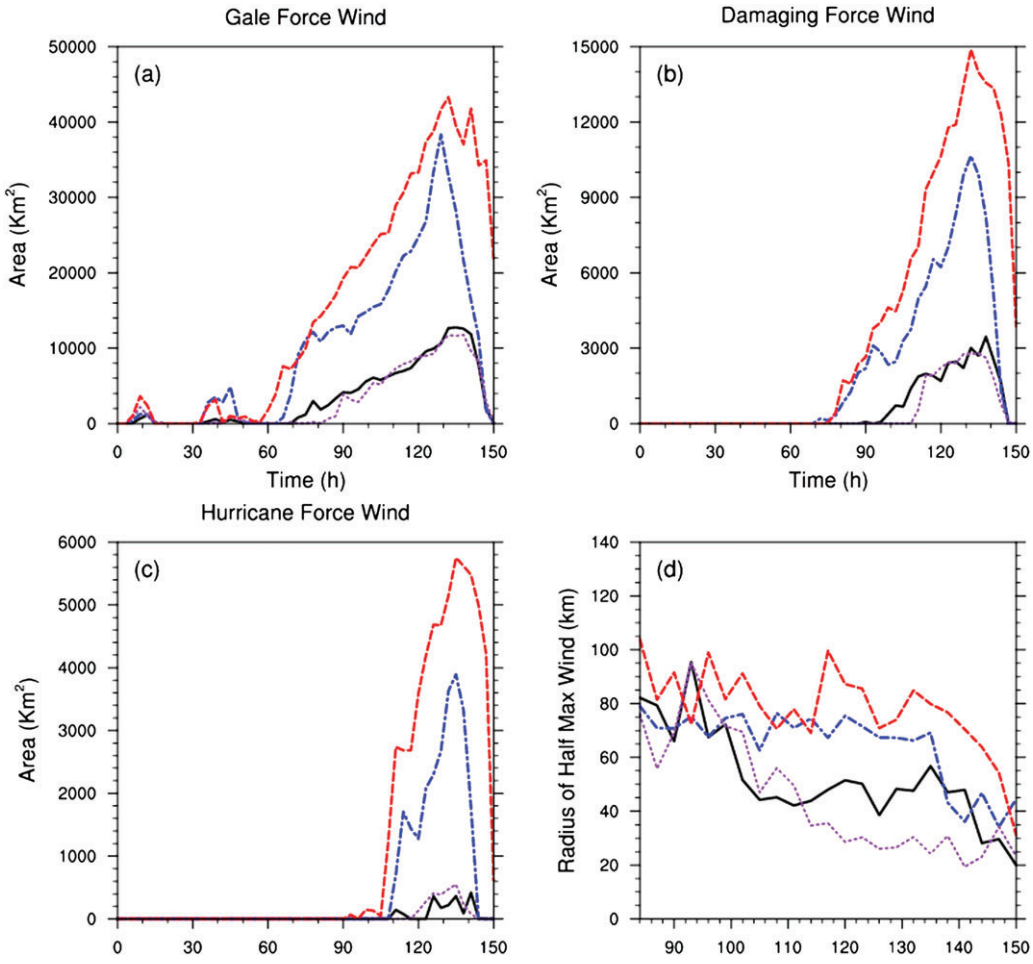

Figure 4. Area of (a) gale-force wind (34 knots or 17.5 m s^{-1}), (b) damaging-force wind (50 knots or 25.7 m s^{-1}) and (c) hurricane-force wind (64 knots or 33 m s^{-1}), calculated for the control experiment (CTL, solid), T1 (dot-dashed), T2 (dashed), and T12 (dotted). (d) shows the radius (km) of half the maximum wind speed for CTL , T1, T2, and T12 (same line styles).

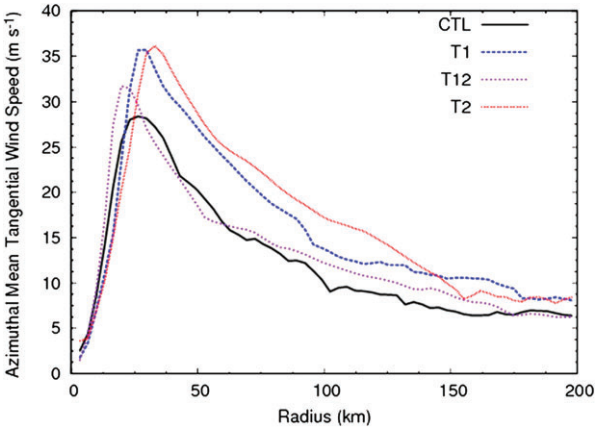

Figure 5. The radial distribution of the azimuthal mean tangential wind speed (m s^{-1}) at the surface, for the control (CTL, solid) and the sensitivity experiments with increased SST and atmospheric temperature profile: T1 (dot-dashed) , T2 (dashed), and T12 (dotted), at the moment of maximum intensity.

similar (Figure 5), larger differences are seen with height. T2 has a substantially enhanced wind speed with height.

Another question is whether the initial TC size is a predictor for the mature size of the cyclone. Figure 2 shows the different TC intensities in terms of maximum surface wind and minimum sea level pressure for each simulation, corresponding to four stages in the cyclone lifetime: initial (0–60 h), development (60–78 h), intensifying stage (78–138 h) and decaying stage or landfall (138–150 h).

Figure 4 shows the vortex size for each of the experiments the control, T1, T2 and T12. After approximately 60 h of integration the cyclone is formed. The initial TC size is defined here as the area of the gale-force winds in all the simulations, therefore we consider the end of the initial stage of the storm to be at 24 March 2004 1200 UTC after 60 h, when the surface wind reaches 17.5 m s^{-1}. The surface pressure drops earlier in T2, 3 h later in T1 and 6 h later in CTL and T12. The key result is that, at the end of the initial stage, the initial vortex size is the largest in T2 and larger in T1 than in the control. T12 has a smaller initial vortex size than the control simulation. Consequently, we find that an initial larger TC size leads to stronger winds and a larger TC size at the mature stage.

3.4. *Latent heat flux*

We now show how the terms in the surface latent heat flux affect the initial and hence the final TC size. Figure 7 shows the average surface latent heat flux (W m^{-2}) for the gale-force wind, damaging-force wind and hurricane-force wind areas. The average latent heat flux is higher in T2 and T1 compared to the control run, while in T12 the flux is slightly reduced. There is a clear linear relation between the average surface latent heat flux and the TC area as diagnosed by all the wind thresholds.

The relative change of the contributing terms in the latent heat flux equation can be inferred from the surface latent heat flux (LHF) bulk aerodynamic formula from Liu *et al.*(1979):

$$LHF = \rho LeCeU(q_s - q_a) = \rho LeCeU\Delta q \qquad (1)$$

where ρ is the density of air, Le is the latent heat of evaporation, Ce is the stability turbulent exchange coefficient for latent heat, and $U$is the average value of the wind speed relative to the sea surface at a height of 10 m; q_s and q_a are the respective sea

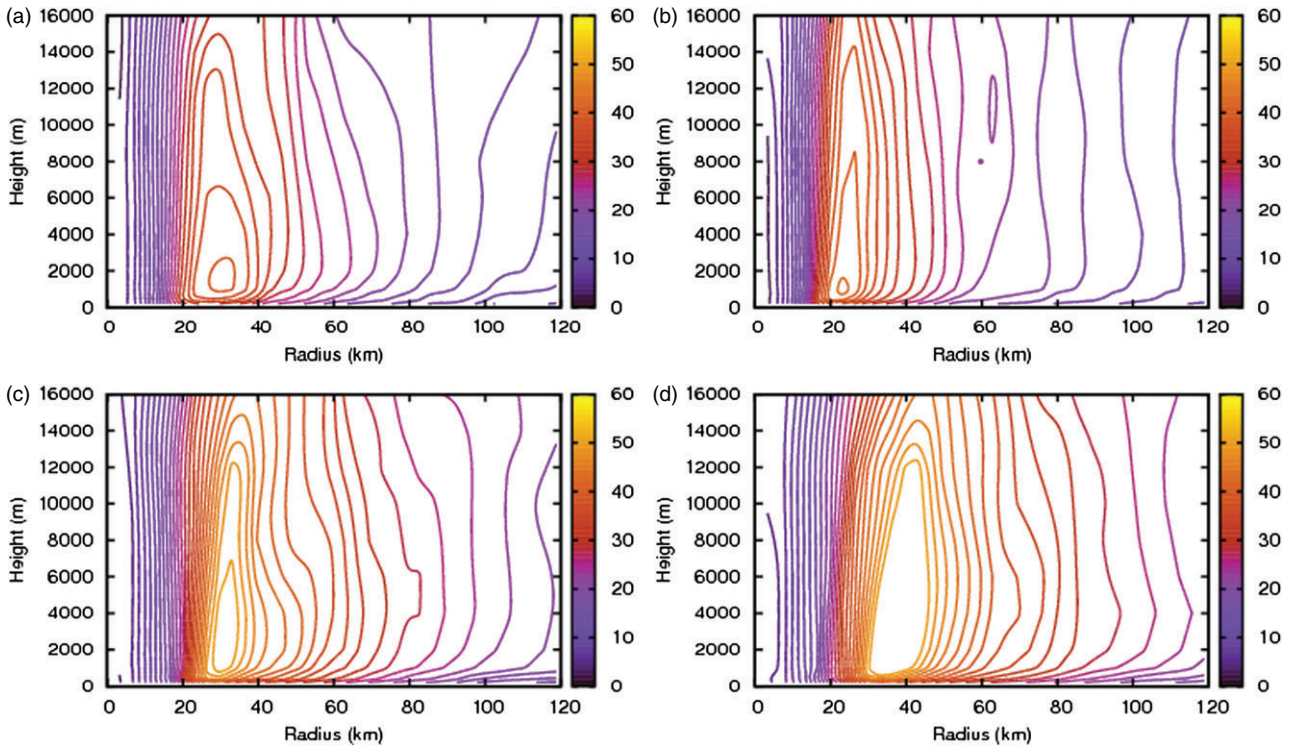

Figure 6. The radius–height profiles of the azimuthal mean tangential wind speed (m s^{-1}) for (a) the control (CTL), and for the sensitivity experiments (b) T12, (c) T1, and (d) T2, at the maximum intensity.

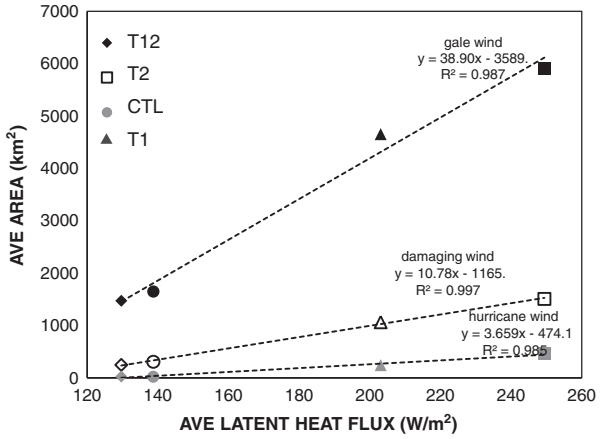

Figure 7. The average surface latent heat flux (W m^{-2}) against averaged area for the gale-force, damaging-force and hurricane-force wind (km^2) calculated in a $3^{\circ} \times 3^{\circ}$box around the centre of the storm.

surface and near-surface atmospheric specific humidity, and the differences betweenq_s and q_a are denoted by Δq. The differences between surface saturation specific humidity and actual surface air specific humidity are different in the experiments. Increased wind speeds will also yield greater latent heat flux. We therefore want to understand the changing contributions of the terms in the flux equation as the cyclone evolves. Thus, we consider $U$and Δq the main contributors in Eq. (1) and we calculate the relative change for each term separately.

Figure 8 shows the relative changes of the differences of the saturation specific humidity at the sea temperature and the air specific humidity at 2 m, and of the average wind speed contributions to the surface latent heat flux for T1 and T2 against CTL. During the initial stage of the storm's lifetime (up to 60 h), there is a predominant contribution from the Δq term to surface latent heat flux in T1, T2 and CTL, while later, during the development, intensification and landfall stages, the surface wind becomes more important and exceeds the contribution coming from the specific humidity difference.

4. Discussion

We have identified that the size of the cyclone is sensitive to temperature. As the temperature increases, it leads to an exponential growth of saturation vapour pressure which has the direct effect of increasing the surface fluxes. We note that may not always be the case, as Lorenz *et al.*(2010) have shown. Here the surface latent heat flux was averaged over the cyclone lifetime. The results show a linear and significant correlation of the increase of TC size with the latent heat flux for all the considered wind thresholds. The latent heat flux relationship is also consistent with the reduced TC size growth in the T12 experiment which has a smaller temperature difference between the ocean and the atmosphere, and boundary layer stabilized in this case.

The surface latent heat flux was identified as an important factor controlling the TC size and we have identified two regimes. In the initial regime, the latent heat flux changes are dominated by humidity gradients and then in the next stage the effect is amplified by the winds (Emanuel, 1986; Molinari *et al.*, 2004). The final TC size is therefore determined by larger initial surface latent heat fluxes and ultimately by increased surface wind. As Xu and Wang (2010a) have shown in an idealized framework, stronger winds will produce larger outer-core entropy fluxes, which will support stronger convection and active spiral rainbands, and diabatic heating, which will contribute to the expansion of the tangential wind fields. This positive feedback causes a larger initial size, and will lead finally to a larger mature TC. Our results are in agreement with this work and also with Rozoff *et al.*(2012), showing that larger surface latent heat flux leads to larger TC size. We also find that initial latent heat flux and the initial vortex size determine the size of the final mature TC, consistent with the results of Xu and Wang (2010b). In the final stages the stronger winds favour larger surface entropy flux and thus more active spiral rainbands, which act as a positive feedback for the initial large TC size driven by the sea–air moisture contrast. Shen *et al.*(2000) and Hill and Lackmann (2011) analysed the sensitivity of TC intensity and size to different initial equilibrium temperature profiles in the Tropics. They showed that the stabilization due to maximized warming in the upper troposphere (near 300 hPa)

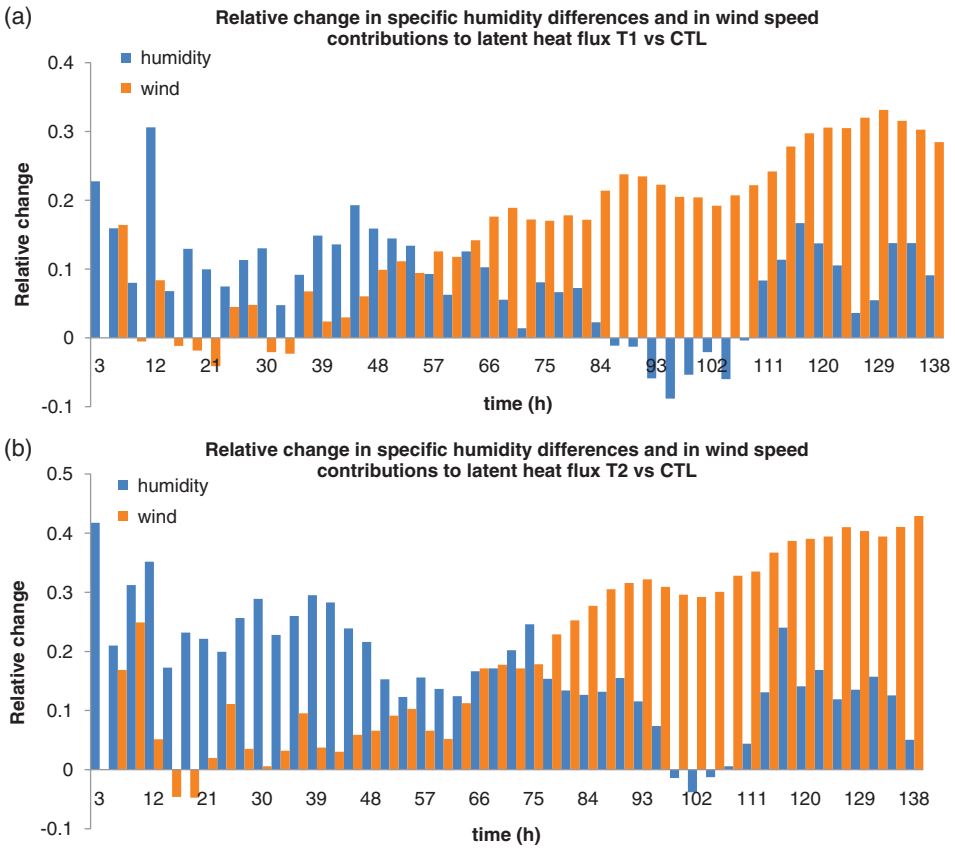

Figure 8. Relative change of difference of the saturation specific humidity at the sea temperature and specific humidity at 2 m and average wind speed contributions to the surface latent heat flux during integration time for (a) the sensitivity experiment with 1 °C increase of atmospheric temperature and SST, T1 versus CTL.; $(\Delta U/\overline{U}$ is the relative change of surface wind speed $\Delta U = U_{SKT1} - U_{CTL}$; $\overline{U} = (U_{SKT1} + U_{CTL})/2$, and $\Delta(\Delta q)/\overline{\Delta q}$ is the relative change of specific humidity difference between sea and air (where $\Delta(\Delta q) = \Delta(q_s - q_a)_{SKT1} - \Delta(q_s - q_a)_{CTL}$; $\overline{\Delta q} = ((q_s - q_a)_{SKT1} + (q_s - q_a)_{CTL})/2$. (b) is as (a), but for T2 with 2 °C increase.

reduces future TC intensification by 50%, while no impact on TC size was found. Equilibrium temperature profiles from climate change projections show amplified warming in the upper troposphere at low latitudes, due to humidity adjustment. This relative warming aloft is reduced in middle to high latitudes, as in our region of interest (Randall *et al.*, 2007). After 1 day, in our experiments the troposphere is also stabilised. In T2 the temperature difference between 300 and 850 hPa is about 1.5 °C higher than the control, as our upper troposphere preferentially warms shortly after initialisation. Therefore, unlike Shen *et al.*(2000), we find increased TC size despite the fact that our initial temperature perturbations increased the upper-tropospheric static stability. Holland and Merrill (1984) pointed out that low-level environmental forcing will directly affect TC size and strength, while an upper-tropospheric environmental forcing will cause changes in intensity and, possibly, in strength.

Weatherford and Gray (1988b) and Chan and Chan (2012) showed that the relationship between intensity and size is weak. Our results here confirm that the relationship is not always simple. A linear increase in radius would be expected to give rise to a squared dependence on area. The winds in T1 and T2 are both stronger (maximum wind by factor 1.2) and cover a larger area (by factor 3.5 for gale force), than in the control. However the difference of sizes between them and T12 and the control cannot simply be explained by maximum wind speed changes. Maximum wind speed is only one variable explaining our size effects.

We note that the larger TC size increases occur even though the potential intensity, as defined by Emanuel (1986), does not change significantly here. Lin *et al.*(2012) propose that potential intensity change may be a proxy for size change. Our results suggest that the size relationship is more complex.

5. Conclusions

Size is an important factor in determining the destructive potential of a tropical cyclone. We have explored, through simulations at high resolution, how the TC size responds to changes of atmospheric and sea surface temperature. We have shown that the TC increases significantly in size, and less in intensity, in the presence of higher SST and atmospheric temperatures. The size effect is affected by the maximum wind speed change, but the two do not have a simple relationship in our experiments. The size effect is novel here for a real cyclone case combining atmosphere and ocean temperature changes. The growth of area increases sharply with the wind threshold. There is a clear linear relationship between the TC size increase and the latent heat flux generated during the TC lifetime. The key finding is that the initial increase in size is caused by the enhanced humidity gradient driving the latent heat flux rather than the wind. In the subsequent development, the contribution from the surface wind dominates the flux and the TC size growth. This study shows that temperature may have profound impact on tropical cyclone size by strongly influencing the early development stages. Further work to analyze complex thermodynamic and dynamic mechanisms controlling the TC size in other cyclone-prone regions is required.

6. Acknowledgements

We thank BP plc Upstream Environmental Technology Program for their support and the referees for their helpful comments.

References

Chan KTF, Chan JCL. 2012. Size and strength of tropical cyclones as inferred from QuikSCAT data. *Mon. Weather Rev.* **140**: 811–824, doi: 10.1175/MWR-D-10-05062.1.

Cocks SB, Gray WM. 2002. Variability of the outer wind profiles of western north Pacific typhoons: Classifications and techniques for analysis and forecasting. *Mon. Weather Rev.* **130**: 1989–2005.
Dean L, Emanuel KA, Chavas DR. 2009. On the size distribution of Atlantic tropical cyclones. *Geophys. Res. Lett.* **36**: L14803, doi: 10.1029/2009GL039051.
Dee DP, Uppala SM, Simmons AJ, Berrisford P, Poli P, Kobayashi S, Andrae U, Balmaseda MA, Balsamo G, Bauer P, Bechtold P, Beljaars ACM, van de Berg L, Bidlot J, Bormann N, Delsol C, Dragani R, Fuentes M, Geer AJ, Haimberger L, Healy SB, Hersbach H, Hólm EV, Isaksen L, Kållberg P, Köhler M, Matricardi M, McNally AP, Monge-Sanz BM, Morcrette J-J, Park B-K, Peubey C, de Rosnay P, Tavolato C, Thépaut J-N, Vitart F. 2011. The ERA-Interim reanalysis: Configuration and performance of the data assimilation system. *Q. J. R. Meteorol. Soc.* **137**: 553–597.
Demuth JL, DeMaria M, Knaff JA. 2006. Improvement of advanced microwave sounding unit tropical cyclone intensity and size estimation algorithms. *J. Appl. Meteorol. Climatol.* **45**: 1573–1581.
Dudhia J. 1989. Numerical study of convection observed during the Winter Monsoon Experiment using a mesoscale two-dimensional model. *J. Atmos. Sci.* **46**: 3077–3107.
Emanuel KA. 1986. An air-sea interaction theory for tropical cyclones. Part I: Steady state maintenance. *J. Atmos. Sci.* **42**: 1062–1071.
Evans J, Braun A. 2012. A climatology of subtropical cyclones in the South Atlantic. *J. Clim.* **25**: 7328–7340, doi: 10.1175/JCLI-D-11-00212.1.
Fisher EL. 1958. Hurricanes and the sea-surface temperature field. *J. Meteorol.* **15**: 328–333.
Hill KA, Lackmann GM. 2009. Influence of environmental humidity on tropical cyclone size. *Mon. Weather Rev.* **137**: 3294–3315.
Hill KA, Lackmann GM. 2011. The impact of future climate change on TC intensity and structure: A downscaling approach. *J. Clim.* **24**: 4644–4661.
Hong SY, Noh Y, Dudhia J. 2006. A new vertical diffusion package with an explicit treatment of entrainment processes. *Mon. Weather Rev.* **134**: 2318–2341.
Holland G, Merrill R. 1984. On the dynamics of tropical cyclone structural changes. *Q. J. R. Meteorol. Soc.* **110**: 723–745.
Kain JS. 2004. The Kain–Fritsch convective parameterization scheme: An update. *J. Appl. Meteorol.* **43**: 170–181.
Kain JS, Fritsch JM. 1993. Convective parameterization for mesoscale models: The Kain–Fritsch scheme. *The Representation of Cumulus Convection in Numerical Models*, Meteorological Monograph **24**: 165–170. American Meteorological Society Boston, MA.
Kimball SK, Mulekar MS. 2004. A 15-year climatology of North Atlantic tropical cyclones. Part I: Size parameters. *J. Clim.* **17**: 3555–3575.
Knapp KR, Kruk MC, Levinson DH, Diamond HJ, Neumann CJ. 2010. The International Best Track Archive for Climate Stewardship (IBTrACS): Unifying tropical cyclone best track data. *Bull. Am. Meteorol. Soc.* **91**: 363–376, doi: 10.1175/2009BAMS2755.1.
Lin N, Emanuel KA, Oppenheimer M, Vanmarcke E. 2012. Physically based assessment of hurricane surge threat under climate change. *Nat. Climate Change* **2**: 462–467, doi: 10.1038/nclimate1389.
Liu KS, Chan JCL. 1999. Size of tropical cyclones as inferred from ERS-1 and ERS-2 data. *Mon. Weather Rev.* **127**: 2992–3001.
Liu WT, Katsaros KB, Businger JA. 1979. Bulk parameterization of air-sea exchanges of heat and water vapor including the molecular constraints at the interface. *J. Atmos. Sci.* **86**: 1722–1735.
Lorenz DJ, DeWeaver ET, Vimont DJ. 2010. Evaporation change and global warming: The role of net radiation and relative humidity. *J. Geophys. Res.* **115**: D20118, doi: 10.1029/2010JD013949.
McTaggart-Cowan R, Bosart L, Davis CA, Atallah EH, Gyakum JR, Emanuel KA. 2006. Analysis of hurricane Catarina (2004). *Mon. Weather Rev.* **134**: 3029–3053.
Merrill RT. 1984. A comparison of large and small tropical cyclones. *Mon. Weather Rev.* **112**: 1408–1418.
Mlawer EJ, Taubman SJ, Brown PD, Iacono MJ, Clough SA. 1997. Radiative transfer for inhomogeneous atmosphere: RRTM, a validated correlated-k model for the longwave. *J. Geophys. Res.* **102**: 16663–16682, doi: 10.1029/97JF00237.
Molinari J, Vollaro D, Corbosiero KL. 2004. Tropical cyclone formation in a sheared environment: A case study. *J. Atmos. Sci.* **61**: 2493–2509.
Pezza AB, Simmonds I, Pereira Filho AJ. 2009. Climate perspective on the large-scale circulation associated with the transition of the first South Atlantic hurricane. *Int. J. Climatol.* **29**: 1116–1130, doi: 10.1002/joc.1757.
Randall DA, Wood RA, Bony S, Colman R, Fichefet T, Fyfe J, Kattsov V, Pitman A, Shukla J, Srinivasan J, Stouffer RJ, Sumi A, Taylor KE. 2007. Climate models and their evaluation. In *Climate Change 2007: The Physical Science Basis. Contribution of Working Group I to the Fourth Assessment Report of the Intergovernmental Panel on Climate Change*, Solomon S, Qin D, Manning M, Chen Z, Marquis M, Averyt KB, Tignor M, Miller HL (eds.). Cambridge University Press: Cambridge, UK and New York, NY; 589–662.
Rotunno R, Emanuel KA. 1987. An air–sea interaction theory for tropical cyclones. Part II: Evolutionary study using a nonhydrostatic axisymmetric numerical model. *J. Atmos. Sci.* **44**: 542–561.
Rozoff CM, Nolan DS, Kossin JP, Zhang F, Fang J. 2012. The roles of an expanding wind field and inertial stability in tropical cyclone secondary eyewall formation. *J. Atmos. Sci.* **69**: 2621–2643, doi: 10.1175/JAS-D-11-0326.1.
Shen W, Tuleya RE, Ginis I. 2000. A sensitivity study of the thermodynamic environment on GFDL model hurricane intensity: Implications for global warming. *J. Clim.* **13**: 109–121, doi: 10.1175/15200442(2000)013>0109:assott<2.0.CO;2.
Skamarock WC, Klemp JB, Dudhia J, Gill DO, Barker DM, Wang W, Powers JG. 2005. 'A description of the advanced research WRF version 2', Technical Note TN-468 STR. NCAR Boulder, CO, 88 pp.
Stovern DR, Ritchie EA. 2012. The importance of atmospheric temperature on the size and structure of tropical cyclones. *Proceedings of 30th AMS Conference on Hurricanes and Tropical Meteorology*, 15–20 April 2012, Ponte Vedra Beach, FL. American Meteorological Society Boston, MA.
Wang Y. 2009. How do outer spiral rainbands affect tropical cyclone structure and intensity? *J. Atmos. Sci.* **66**: 1250–1273.
Weatherford CL, Gray WM. 1988a. Typhoon structure as revealed by aircraft reconnaissance. Part I: Data analysis and climatology. *Mon. Weather Rev.* **116**: 1032–1043.
Weatherford CL, Gray WM. 1988b. Typhoon structure as revealed by aircraft reconnaissance. Part II: Structural variability. *Mon. Weather Rev.* **116**: 1044–1056.
Xu J, Wang Y. 2010a. Sensitivity of tropical cyclone inner-core size and intensity to the radial distribution of surface entropy flux. *J. Atmos. Sci.* **67**: 1831–1852.
Xu J, Wang Y. 2010b. Sensitivity of the simulated tropical cyclone inner-core size to the initial vortex size. *Mon. Weather Rev.* **138**: 4135–4157.

